Experimental Demonstration of Spontaneous Chirality in a Nonlinear Microresonator

Qi-Tao Cao, Heming Wang, Chun-Hua Dong, Hui Jing, Rui-Shan Liu, Xi Chen, Li Ge, Qihuang Gong, and Yun-Feng Xiao

Phys. Rev. Lett. **118**, 033901 — Published 17 January 2017

DOI: 10.1103/PhysRevLett.118.033901

Experimental demonstration of spontaneous chirality in a nonlinear microresonator

Qi-Tao Cao[1], Heming Wang[1], Chun-Hua Dong[2], Hui Jing[3], Rui-Shan Liu[1], Xi Chen[1], Li Ge[4,5], Qihuang Gong[1,6], and Yun-Feng Xiao[1,6]*

[1] *State Key Laboratory for Mesoscopic Physics and School of Physics, Peking University; Collaborative Innovation Center of Quantum Matter, Beijing 100871, P. R. China*

[2] *Key Laboratory of Quantum Information, University of Science and Technology of China, Hefei 230026, P. R. China*

[3] *Key Laboratory of Low-Dimensional Quantum Structures and Quantum Control of Ministry of Education, Department of Physics and Synergetic Innovation Center for Quantum Effects and Applications, Hunan Normal University, Changsha 410081, China*

[4] *Department of Engineering Science and Physics, College of Staten Island, CUNY, Staten Island, New York 10314, USA*

[5] *The Graduate Center, CUNY, New York, NY 10016, USA and*

[6] *Collaborative Innovation Center of Extreme Optics, Taiyuan 030006, Shanxi, P. R. China*

(Dated: December 19, 2016)

Chirality is an asymmetric property widely found in nature. Here, we propose and demonstrate experimentally spontaneous emergence of chirality in an on-chip ultrahigh-Q whispering-gallery microresonator, without broken parity or time-reversal symmetry. This counter-intuitive effect arises due to the inherent Kerr-nonlinearity-modulated coupling between clockwise and counterclockwise propagating waves. Above an input threshold of a few hundred microwatts, the initial chiral symmetry is broken spontaneously, and the counter-propagating output ratio exceeds 20:1 with bi-directional inputs. The spontaneous chirality in an on-chip microresonator holds great potential in studies of fundamental physics and applied photonic devices.

Spontaneous chiral symmetry breaking, a phenomenon where mirror-symmetric dynamic laws produce stationary states that violate this symmetry, is a ubiquitous property in nature and diverse fields of modern physics [1], which has been studied extensively, for instance, in Higgs physics [2], double-well Bose-Einstein condensates [3], topological insulators and superconductors [4]. However, spontaneous chiral symmetry breaking has been elusive experimentally in the optical domain, especially for micro- and nano-photonics. Such setup usually demands multiple identical subsystems such as photonic nanocavities [5], meta-molecules [6] and other dual-core settings [7, 8]. As a prominent photonic device, the ultrahigh-Q whispering-gallery mode (WGM) microresonator is widely used for applications such as strong-coupling cavity quantum electrodynamics, cavity optomechanics, ultralow-threshold lasers to highly sensitive sensing [9]. In a practical WGM resonator, the clockwise (CW) and counterclockwise (CCW) propagating waves are coupled to each other due to the backscattering, leading to symmetric and antisymmetric standing-wave modes with equal CW and CCW amplitudes [10–12]. While this chiral symmetry can be broken locally by wave effects such as the Goos-Hänshen shift and Fresnel filtering for certain regions of an optical mode [13, 14], the demonstrations of overall chirality have to rely on external perturbations to a resonator, either by breaking the parity [15–20] or time-reversal [21–23] symmetry.

The chirality with unbalanced CW and CCW components not only attracts general interest in physics, but also is of importance in novel devices such as unidirectional-emission microlasers [13–15], optical gyroscopes [17, 22, 23], and single-particle detection [16, 18].

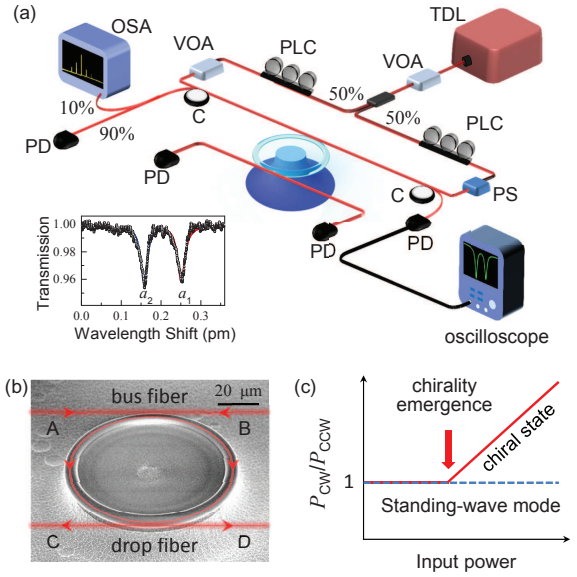

FIG. 1. (Color) (a) A toroidal microcavity is evanescently side coupled by two tapered fiber waveguides. Inset: a typical transmission spectrum collected by port B. TDL: tunable diode laser; PLC: polarization controller; VOA: variable optical attenuator; PS: phase shifter; C: circulator; OSA: optical spectroscope analyzer; PD: photodetector. (b) Scanning electron microscope image of the silica microtoroid. Ports A and B of the bus fiber waveguide excite WGMs, and ports C and D of the drop fiber waveguide collect the emission of CW and CCW components separately. (c) Schematic illustration of CW to CCW intensity ratio for a standing wave mode (blue) and a CW chiral state (red), as the input power increases.

In this paper, we experimentally demonstrate the spontaneous emergence of chirality induced by Kerr nonlinear-

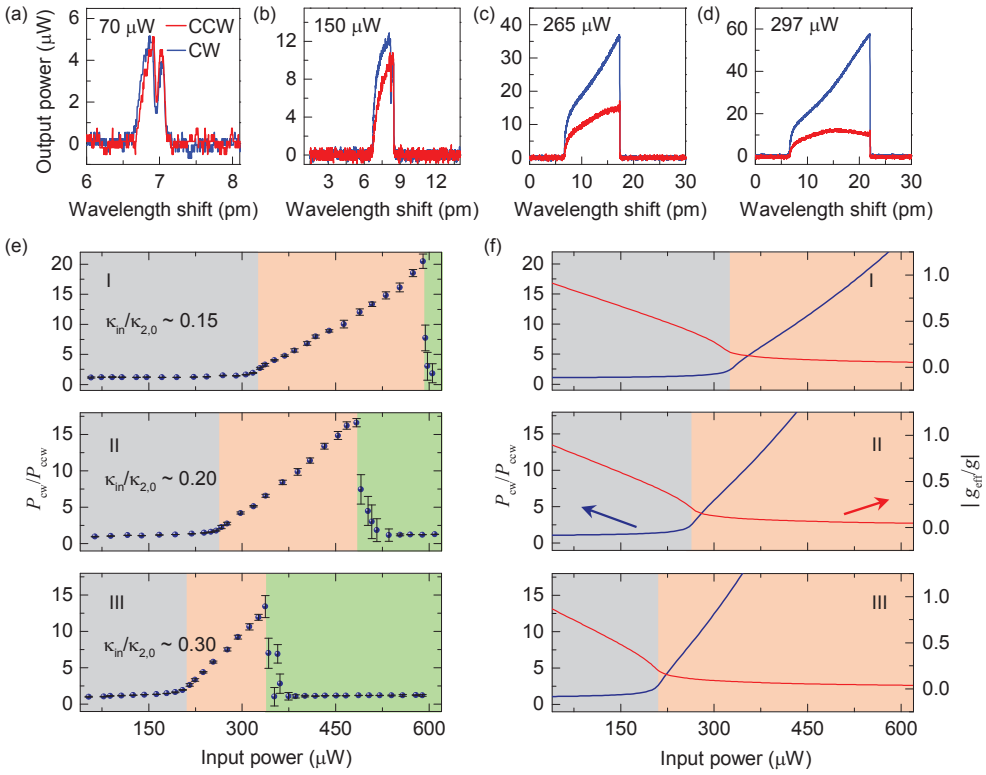

FIG. 2. (Color) (a)-(d) CW (blue) and CCW (red) output spectra collected by the drop fiber under the inputs of 70, 150, 265 and 297 μW from port A only. (e) The experimental intensity ratio $\mathfrak{R} = P_{\rm cw}/P_{\rm ccw}$ versus the input power, with $\kappa_{\rm in}/\kappa_{2,0} \approx 0.15$, 0.20 and 0.30, from top to bottom. (f) The theoretical $\mathfrak{R}$ (blue curve) and the scaled effective coupling strength $|g_{\rm eff}/g|$ (red curve) under the same experimental condition in (e). Parameters: $2g/2\pi = 11.67$ MHz, $\kappa_{2,0}/2\pi = 2.93$ MHz, and $M = 3.64\times10^{11}\,{\rm J}^{-1}$. In (e) and (f) the shaded regions indicate standing wave mode regime (gray), chiral state regime (orange) and four-wave mixing regime (green).

ity in a single ultrahigh-Q WGM microresonator (Fig. 1) without any explicit breaking of parity or time-reversal symmetry. Our theoretical analysis reveals the physical mechanism of this intriguing effect: the Kerr nonlinearity gives rise to an intensity-dependent CW-CCW coupling that becomes approximately zero beyond a threshold, causing one of the standing-wave modes to become unstable and spontaneously evolve into a chiral state as schematically illustrated in Fig. 1(c).

As shown in Figs. 1(a) and (b), a silica toroidal microresonator with a principal (minor) diameter of 78 μm (6.8 μm) is side coupled by a bus and a drop fiber waveguide. In the 1550 nm wavelength band, the transmission spectrum of transverse-electric (TE) polarization from port A to B shows two nearby TE resonances with ultrahigh quality factors ($Q \sim 7.8\times10^7$), i.e., a low-frequency symmetric mode a_1 and a high-frequency antisymmetric mode a_2, exhibiting the strong intrinsic modal coupling between CW and CCW waves [inset of Fig. 1(a)] [11]. Under the input from the bus fiber, the intensities of CW and CCW components are measured by the drop fiber, with the same coupling rate. Note that for a weak input power, each mode of this doublet is chiral symmetric containing equal amounts of CW and CCW components [Fig. 2(a)], which does not depend on the input direction.

With input from port A only, we analyze the spectra of the intensities collected by the drop fiber [Figs. 2(b)-(d)] for the antisymmetric mode a_2. Although these spectra no longer have a Lorentzian shape due to the thermal effect and Kerr nonlinearity [24] when the input power is increased, the growing imbalance between the CW and CCW components is readily seen, which is not expected from thermal effects alone [25]. To be quantitative, we characterize the chirality by $\mathfrak{R} = P_{\rm cw}/P_{\rm ccw}$, where $P_{\rm cw}$ ($P_{\rm ccw}$) is the on-resonance output power of the CW (CCW) component. It is evident that $\mathfrak{R}$ shows a threshold behavior as the input power increases, as shown in Fig. 2(e) I-III. For example, $\mathfrak{R}$ is near unity with the input power from 40 μW to 260 μW in Fig. 2(e) II, and it increases rapidly afterwards. Here, a forward propagating waveguide mode is much more likely to excite the CW chiral state with $\mathfrak{R} > 1$ compared to the CCW chiral state because of momentum conservation. By switching the input to port B, the CCW chiral state with $\mathfrak{R} < 1$ can also be observed (not shown). We note that the sudden drop of $\mathfrak{R}$ with a higher input power is due to four-

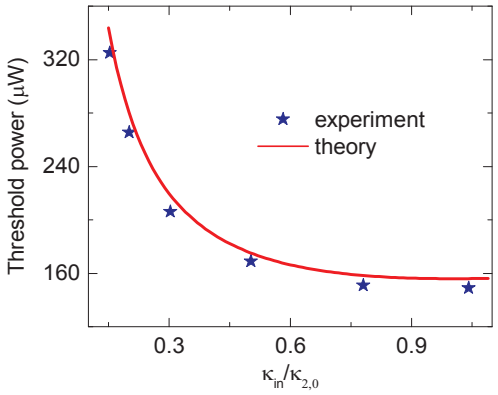

FIG. 3. (Color) Dependence of chirality thresholds on the coupling rates $\kappa_{\rm in}$. Blue stars and red curves show experimental data and analytical results, respectively. Parameters are the same as in Fig. 2(f).

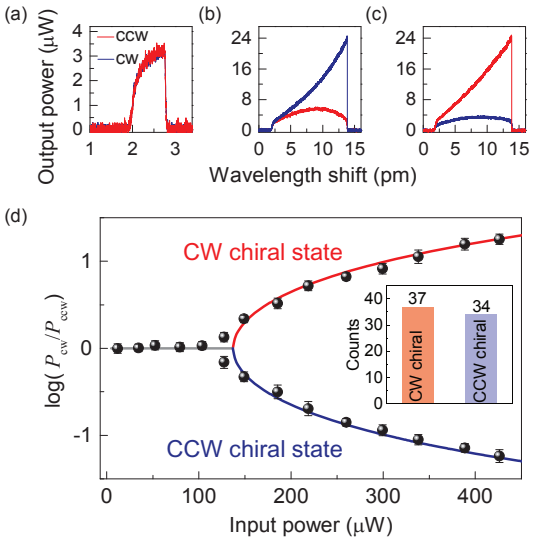

FIG. 4. (Color) (a) Typical drop-port spectrum of the antisymmetric mode, with a total input power of 103 μW from ports A and B. A chiral symmetric state is observed. (b)-(c) Same as (a) but with a total input power of 338 μW. The CW and CCW chiral states are observed, respectively. (d) Dependence of log$\Re$ on the total input power. The solid curves are theoretical results for a lossy resonator with the bifurcation, and the black dots are the corresponding experimental data. Parameters: $\kappa_{\rm in}/\kappa_{2,0} \approx 0.33$, the rest are the same as in Fig. 2(f). Inset shows the statistics of 71 events of spontaneous symmetry breaking measured under different powers.

wave mixing (FWM) [25]. This spontaneous chirality is found to be universal in our system. More specifically, this qualitative behavior is independent of the coupling rate $\kappa_{\rm in}$ between the bus fiber and the microresonator at the weak input power. The $\kappa_{\rm in}$ varies from sample to sample by adjusting the gap width between the fiber and the cavity, but the threshold behavior of $\Re$ persists as we show in Figs. 2(e) I-III.

We further note that the threshold power increases as the bus fiber-cavity coupling rate decreases (Fig. 3), so does the power range of chiral states before the emergence of FWM [25]. The latter leads to a higher maximal value of $\Re$ at a lower $\kappa_{\rm in}$, which reaches about 20 when $\kappa_{\rm in}/\kappa_{2,0} \approx 0.15$, where $\kappa_{2,0}$ is the intrinsic loss rate of the antisymmetric mode a_2. We note that the fiber coupling efficiency η also displays a qualitative change at the input power of chirality threshold [25]. The η is defined by the depth of normalized transmission dips, and the latter shows the same broadening and distortion with increased power as the intensity spectra collected in the bus fiber. A notable difference from previous studies [24] is that the on-resonance coupling becomes stronger [25].

Up to now we have demonstrated how the one-sided input can excite modes with chiral symmetry, and then break such symmetry when the input power is increased. We note that the one-sided input may cause $\Re$ to differ slightly from 1 when input power is low, but the deviation is very small ($|\Re - 1| < 0.1$) as shown in experiments. To verify that the large observed chirality really does not originate from the asymmetry introduced by the one-sided input, we have also excited the antisymmetric mode using two-sided input from ports A and B [Fig. 1(a)] simultaneously, with identical power and polarization. As can be seen from Fig. 4(a), at low input powers the drop power is symmetric. With the growth of the input power, however, the cavity mode randomly enters a CW [Fig. 4(b)] or a CCW [Fig. 4(c)] chiral state, and $\Re$ shows a bifurcation behavior [Fig. 4(d)]. Neither of the two opposite-direction chiral states shows any statistical preference when 71 events of spontaneous symmetry breaking are analyzed [inset of Fig. 4(d)]: their difference (3 events) falls within the standard deviation (4.2 for 71 events) of a binomial distribution with equal likelihood. We note that by changing the relative phase of input, the symmetric mode can also be excited, which retains its symmetry and $\Re \approx 1$ even at high power levels [25].

We now analyze the mode dynamics of a lossless cavity by introducing Kerr nonlinearity. The Hamiltonian of the cavity reads [25] $H = \hbar g(a_2^\dagger a_2 - a_1^\dagger a_1) - \frac{1}{4}(M\hbar\omega)\hbar g(\delta_{\mu\nu}\delta_{\rho\sigma} + \delta_{\mu\sigma}\delta_{\nu\rho} + \delta_{\mu\rho}\delta_{\nu\sigma})a_\mu^\dagger a_\rho^\dagger a_\nu a_\sigma$, where g is the intrinsic linear coupling strength between CW and CCW waves, ω is the mode frequency, δ is the Kronecker delta, and repeated indices are summed over. The coefficient M is proportional to the scalar Kerr nonlinear susceptibility $\chi^{(3)}$. In the CW-CCW basis $a_{\rm cw} = (a_1 + ia_2)/\sqrt{2}$ and $a_{\rm ccw} = (a_1 - ia_2)/\sqrt{2}$, the coupled-mode equations read

$$\frac{1}{ig}\frac{da_m}{dt} = M(|a_m|^2 + |a_{m'}|^2)a_m + (1 + Ma_{m'}^* a_m)a_{m'}, \quad (1)$$

where m and m' ($m \neq m'$) stand for CW and CCW. Here the third term $iga_{m'}$ represents linear coupling, the first term $igM|a_m|^2 a_m$ represents self-phase modulation,

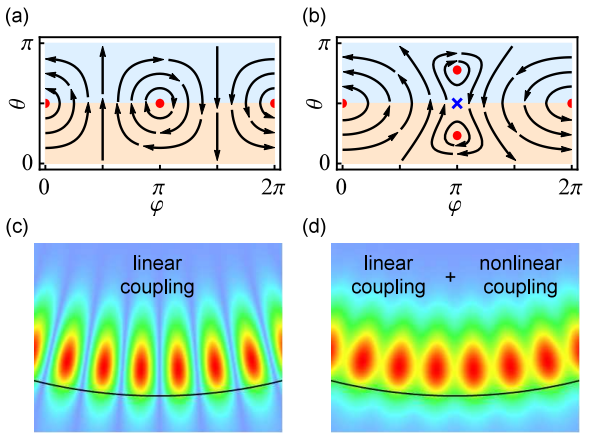

FIG. 5. (Color) (a)-(b) Trajectories of state evolutions for $MA^2 = 0,\ 3$ in the phase space. States dominated by the CCW (CW) wave components lie in the upper blue-shaded area (lower orange-shaded area), with $\pi/2 < \theta \leq \pi$ ($0 \leq \theta < \pi/2$). Red dots (blue cross) mark stable (unstable) states. (c)-(d) Patterns of the antisymmetric standing-wave mode and the chiral state obtained from two-dimensional numerical simulations [25]. In (c), there is only linear coupling between CW and CCW components, while in (d) the nonlinear coupling is present.

and the second and fourth terms $2igM|a_{m'}|^2 a_m$ represent cross-phase modulation, which reflects the fact that cross-phase modulation induces twice the refractive index change compared to self-phase modulation. For convenience, the state amplitudes can be written in terms of the Bloch sphere parameters, $a_{\rm cw} \equiv Ae^{i\alpha}\cos(\theta/2)$ and $a_{\rm ccw} \equiv Ae^{i\alpha}\sin(\theta/2)e^{i\varphi}$, where $Ae^{i\alpha}$ is the total complex amplitude, and $0 \leq \theta \leq \pi$ and $0 \leq \varphi \leq 2\pi$ describe the relative amplitude and phase difference of the two propagating waves, which can be used to study the evolution of states and existing modes. As shown in Fig. 5, the CW and CCW amplitudes of the states oscillate because of the intrinsic coupling. In the case of $MA^2 = 0$ where the nonlinear effects are turned off [Fig. 5(a)], the trajectories circulate around the red dots at $\theta = \pi/2$, $\varphi = 0$ and $\theta = \pi/2$, $\varphi = \pi$. The former fixed point corresponds exactly to the symmetric mode a_1 while the latter to the antisymmetric mode a_2. After the intensity increases to $MA^2 = 2$, a pitchfork bifurcation occurs and two new steady states emerge [e.g., Fig. 5(b) at $MA^2 = 3$]. These states (marked as two red dots at $\varphi = \pi$) gain chirality spontaneously, while the mode a_2 at $\theta = \pi/2$, $\varphi = \pi$ (marked as a blue cross) becomes unstable.

As suggested by Eq. (1), the coupling between the CW and CCW waves consists of both the linear intrinsic coupling and the nonlinear intermodal interaction resulting in an *intensity-dependent* effective coupling coefficient $g_{\rm eff} \equiv (1 + Ma^*_{\rm ccw}a_{\rm cw})g$. Considering the optical Kerr effect, the standing-wave modes can be considered as periodic potentials along the microcavity perimeter. In this regard, the propagating waves are reflected by the nonlinearity-related potential, adding coherently to the linear coupling. With a low intracavity intensity, the nonlinear modulation on the refractive index is weak, and $g_{\rm eff} \sim g > 0$, resulting in the clear standing wave pattern as usual [Fig. 5(c)]. With a strong enough intensity above the threshold $A^2 = 2M^{-1}$, the coupling between the propagating waves is canceled effectively, i.e., $g_{\rm eff} = 0$, under the phase-matching condition $\varphi = \pi$ satisfied by the antisymmetric mode. In this case, bifurcation occurs and the original antisymmetric mode becomes unstable. The chiral symmetry is broken, with a much reduced interference pattern, instead of a standard standing wave [Fig. 5(d)]. A stronger intensity leads to a greater chirality. For the low-frequency mode a_1 corresponding to $\varphi = 0$, however, the coupling is enhanced by the nonlinear effects, i.e., $g_{\rm eff} > g$, and no chirality can be found near this mode.

In a real system, $\mathfrak{R}$ can be derived from Eq. (1) with losses and input terms using a perturbative approach [25]. Figures 2(f) and 4(d) plot $\mathfrak{R}$ as a function of the input power, with mode parameters obtained from experiments. It is found that the experimental results are in good agreement with the theory until FWM appears. For instance, at the threshold value of 260 μW in Figs. 2(f) II, the bifurcation occurs and the chiral symmetry is broken spontaneously, where $|g_{\rm eff}|$ decreases to zero. Theoretically, when no Kerr nonlinearity is present, the one-sided input will lead to a slight bias of $\mathfrak{R}$ from 1, but such minor asymmetry as a linear response does not vary with input power, and an $\mathfrak{R}$ exceeding 20 is a direct result of spontaneous chiral symmetry breaking induced by nonlinear effects.

In summary, we have demonstrated the Kerr nonlinearity-induced spontaneous chirality with unbalanced CW and CCW components in a single microresonator, without any explicit breaking of parity or time-reversal symmetry. This spontaneous chirality is different from the unidirectional ring laser which relies on carrier concentration and mode competition [26–28]. We also note that our chirality threshold is not at an exceptional point [29], which would otherwise introduce a square root singularity to the eigenvalues of the effective Hamiltonian represented by Eq. (1). The latter, however, is not the case [25], hence the pitchfork bifurcation at the chirality threshold, though seemingly identical to parity-time symmetry breaking [30], is caused by a very different mechanism. Furthermore, although the chirality vanishes once the input power is strong enough to generate side bands via FWM, the latter can be suppressed by delicate designs of the cavity geometry.

Q.-T. C. would like to thank L. Wang, S.-X. Zhang and X.-C. Yu for the generous help. This project was supported by the Ministry of Science and Technology of China (Grant No. 2016YFA0301302, 2013CB921904 and 2013CB328704) and the NSFC (Grant No. 61435001,

11474011 and 11654003). H. W., X. C. and R.-S. L. were supported by the National Fund for Fostering Talents of Basic Science (Grant No. J1030310 and J1103205). L.G. acknowledges partial support by the NSF under Grant No. DMR-1506987. Q.-T. C., H. W. and C.-H. D. contributed equally to this work. Q.-T. C. and C.-H. D. performed the experiment. H. W. built the theoretical model. Y.-F. X. designed the experiment and supervised the project. All authors contributed to the discussion, analyzed the data and wrote the manuscript.

Note added.–We would like to draw the reader's attention to a related recent work [31].

* Corresponding author: yfxiao@pku.edu.cn; URL: www.phy.pku.edu.cn/∼yfxiao/

[1] B. A. Malomed, *Spontaneous Symmetry Breaking, Self-Trapping, and Josephson Oscillations* (Springer, 2013).
[2] M. Endres, T. Fukuhara, D. Pekker, M. Cheneau, P. Schauβ, C. Gross, E. Demler, S. Kuhr, and I. Bloch, Nature **487**, 454 (2012).
[3] T. Zibold, E. Nicklas, C. Gross, and M. K. Oberthaler, Phys. Rev. Lett. **105**, 204101 (2010).
[4] K. Matano, M. Kriener, K. Segawa, Y. Ando, and G.-q. Zheng, Nat. Phys. **12**, 852 (2016).
[5] P. Hamel, S. Haddadi, F. Raineri, P. Monnier, G. Beaudoin, I. Sagnes, A. Levenson, and A. M. Yacomotti, Nat. Photon. **9**, 311 (2015).
[6] M. Liu, D. A. Powell, I. V. Shadrivov, M. Lapine, and Y. S. Kivshar, Nat. Commun. **5**, 4441 (2014).
[7] P. Kevrekidis, Z. Chen, B. Malomed, D. Frantzeskakis, and M. Weinstein, Phys. Lett. A **340**, 275 (2005).
[8] A. W. Snyder, D. Mitchell, L. Poladian, D. R. Rowland, and Y. Chen, J. Opt. Soc. Am. B **8**, 2102 (1991).
[9] H. Cao and J. Wiersig, Rev. Mod. Phys. **87**, 61 (2015).
[10] M. L. Gorodetsky, A. D. Pryamikov, and V. S. Ilchenko, J. Opt. Soc. Am. B **17**, 1051 (2000).
[11] T. Kippenberg, S. Spillane, and K. Vahala, Opt. Lett. **27**, 1669 (2002).
[12] A. Mazzei, S. Götzinger, L. d. S. Menezes, G. Zumofen, O. Benson, and V. Sandoghdar, Phys. Rev. Lett. **99**, 173603 (2007).
[13] Q. Song, L. Ge, A. Stone, H. Cao, J. Wiersig, J.-B. Shim, J. Unterhinninghofen, W. Fang, and G. Solomon, Phys. Rev. Lett. **105**, 103902 (2010).
[14] B. Redding, L. Ge, Q. Song, J. Wiersig, G. S. Solomon, and H. Cao, Phys. Rev. Lett. **108**, 253902 (2012).
[15] G. Chern, H. Tureci, A. D. Stone, R. Chang, M. Kneissl, and N. Johnson, Appl. Phys. Lett. **83**, 1710 (2003).
[16] J. Wiersig, Phys. Rev. Lett. **112**, 203901 (2014).
[17] R. Sarma, L. Ge, J. Wiersig, and H. Cao, Phys. Rev. Lett. **114**, 053903 (2015).
[18] B. Peng, Ş. K. Özdemir, M. Liertzer, W. Chen, J. Kramer, H. Yılmaz, J. Wiersig, S. Rotter, and L. Yang, Proc. Natl. Acad. Sci. **113**, 6845 (2016).
[19] I. Shomroni, S. Rosenblum, Y. Lovsky, O. Bechler, G. Guendelman, and B. Dayan, Science **345**, 903 (2014).
[20] C. Junge, D. O'Shea, J. Volz, and A. Rauschenbeutel, Phys. Rev. Lett. **110**, 213604 (2013).
[21] Z. Wang, Y. Chong, J. Joannopoulos, and M. Soljačić, Nature **461**, 772 (2009).
[22] L. Ge, R. Sarma, and H. Cao, Optica **2**, 323 (2015).
[23] J. Kim, M. C. Kuzyk, K. Han, H. Wang, and G. Bahl, Nat. Phys. **11**, 275 (2015).
[24] T. Carmon, L. Yang, and K. Vahala, Opt. Express **12**, 4742 (2004).
[25] Please refer to the supplementary materials for details, which includes [32–45].
[26] M. Sorel, G. Giuliani, A. Scirè, R. Miglierina, S. Donati, and P. Laybourn, IEEE J. Quantum Electron. **39**, 1187 (2003).
[27] S. V. Zhukovsky, D. N. Chigrin, and J. Kroha, Phys. Rev. A **79**, 033803 (2009).
[28] S. Burkhardt, M. Liertzer, D. O. Krimer, and S. Rotter, Phys. Rev. A **92**, 013847 (2015).
[29] J. Okolowicz, M. Ploszajczak, and I. Rotter, Phys. Rep. **374**, 271 (2003).
[30] C. M. Bender and S. Boettcher, Phys. Rev. Lett. **80**, 5243 (1998).
[31] L. Del Bino, J. M. Silver, S. L. Stebbings, and P. Del'Haye, arXiv:1607.01194 (2016).
[32] Y. K. Chembo and N. Yu, Phys. Rev. A **82**, 033801 (2010).
[33] X. Yang and C. W. Wong, Opt. Express **15**, 4763 (2007).
[34] K. Hayata and M. Koshiba, J. Opt. Soc. Am. B **9**, 1362 (1992).
[35] B. Maes, M. Soljacic, J. D. Joannopoulos, P. Bienstman, R. Baets, S.-P. Gorza, and M. Haelterman, Opt. Express **14**, 10678 (2006).
[36] T. Kippenberg, S. Spillane, and K. Vahala, Phys. Rev. Lett. **93**, 083904 (2004).
[37] M. Han and A. Wang, Opt. Lett. **32**, 1800 (2007).
[38] L. He, Y.-F. Xiao, C. Dong, J. Zhu, V. Gaddam, and L. Yang, Appl. Phys. Lett. **93**, 201102 (2008).
[39] D. Armani, T. Kippenberg, S. Spillane, and K. Vahala, Nature **421**, 925 (2003).
[40] P. Del'Haye, A. Schliesser, O. Arcizet, T. Wilken, R. Holzwarth, and T. Kippenberg, Nature **450**, 1214 (2007).
[41] A. A. Savchenkov, A. B. Matsko, D. Strekalov, M. Mohageg, V. S. Ilchenko, and L. Maleki, Phys. Rev. Lett. **93**, 243905 (2004).
[42] S. Spillane, T. Kippenberg, and K. Vahala, Nature **415**, 621 (2002).
[43] B.-B. Li, W. R. Clements, X.-C. Yu, K. Shi, Q. Gong, and Y.-F. Xiao, Proc. Natl. Acad. Sci. **111**, 14657 (2014).
[44] T. Carmon and K. J. Vahala, Nat. Phys. **3**, 430 (2007).
[45] D. Farnesi, A. Barucci, G. Righini, S. Berneschi, S. Soria, and G. N. Conti, Phys. Rev. Lett. **112**, 093901 (2014).